

# 1 **A thermodynamic model for feldspars in** 2 **KAlSi<sub>3</sub>O<sub>8</sub>–NaAlSi<sub>3</sub>O<sub>8</sub>–CaAl<sub>2</sub>Si<sub>2</sub>O<sub>8</sub> for mineral equilibrium** 3 **calculations**

4 Tim JB Holland<sup>1</sup>, Eleanor CR Green<sup>2</sup> & Roger Powell<sup>2</sup>

5 <sup>1</sup>Department of Earth Sciences, University of Cambridge, Cambridge, UK

6 <sup>2</sup>School of Geography, Earth and Atmospheric Sciences, The University of Melbourne,  
7 Victoria 3010, Australia

8 Corresponding author: [tjbh@cam.ac.uk](mailto:tjbh@cam.ac.uk)

9 **Short title:** Thermodynamic model for feldspars

## 10 **Abstract**

11 Activity-composition ( $a$ - $x$ ) relations for feldspars for petrological calculations in  
12 KAlSi<sub>3</sub>O<sub>8</sub>–NaAlSi<sub>3</sub>O<sub>8</sub>–CaAl<sub>2</sub>Si<sub>2</sub>O<sub>8</sub> are calibrated using literature data for (i) plagioclase  
13 cation-exchange experiments at 600 and 700°C, (ii) experimental ternary feldspar pairs at  
14 880 – 900°C, (iii) the alkali feldspar solvus, and (iv) the dry melting loop for plagioclase.  
15 The results are tested against the calorimetric heat of solution data and the experimental  
16 pressures for plagioclase coexisting with grossular, wollastonite and quartz. As the aim is to  
17 produce  $a$ - $x$  relations suitable for petrological modelling, we do not attempt to model  
18 complex structural phenomena in feldspar, except where they appear to contribute  
19 significantly to the energetics of high-temperature mixing. Seven models were investigated,  
20 using various formulations of entropy of mixing together with the van Laar model for  
21 non-ideal mixing. The model (4TR) that most satisfactorily reproduces the experimental  
22 data is one in which Al and Si partially order onto the four tetrahedral sites, approximated  
23 by reducing the tetrahedral site entropy of mixing by a factor of four. When combined with  
may lead to differences between this version and the Version of Record. Please cite this article  
as doi: [10.1111/jmg.12639](https://doi.org/10.1111/jmg.12639)

24 an ordered albite this model allows a peristerite gap closing at 600°C at the albite  
25 composition. The resulting activity-composition relations for feldspar should be applicable  
26 in petrological phase equilibrium calculations over a large range of geologically-relevant  
27 pressure and temperature.

28 **KEYWORDS** feldspars, activity-composition relations, equilibrium thermodynamics

# 1 Introduction

Feldspars are ubiquitous in crustal and uppermost mantle rocks, so it is of fundamental importance that petrological phase equilibrium modelling should approximate their thermodynamics appropriately. Yet the plagioclase solid solution shows exceptional structural complexity, including phase transitions, extensive short-range order, and “long-range order” (aperiodic, incommensurate ordering), and is still being characterised by mineralogical experiments (e.g. Jin *et al.*, 2019; Jin & Xu, 2017; McConnell, 2008; Carpenter, 1994; Carpenter & McConnell, 1984).

Numerous thermodynamic models have been proposed that reflect at least part of the complexity of structural change across the plagioclase solid solution (e.g. Ghiorso 1984, Green & Usdansky 1986, Fuhrman & Lindsley 1988, Elkins & Grove 1990, Holland & Powell 1992, Holland & Powell 2003, Benisek *et al.* 2010). For example, Holland & Powell (1992) represented the  $C\bar{1}-I\bar{1}$  transition, using two models that were made contiguous at the transition.

In this paper we revisit the modelling of plagioclase for phase equilibrium calculations. Since our purpose is petrological modelling, we seek a simple model. Our goal is not primarily to represent the complexity of feldspar structures – in this case the simpler models (see below) can describe the mixing properties as well as or better than the more complex ones investigated. We require our model to satisfy the following key experimental constraints: (a) experimental cation-exchange data for plagioclase- (NaCl-CaCl<sub>2</sub>) fluid (Orville 1972, Schliestedt & Johannes 1990); (b) alkali feldspar solvus at various pressures (Orville 1963, Luth & Tuttle 1966, Goldsmith & Newton 1974); (c) experimental ternary feldspar pairs (Elkins & Grove 1990); and (d) the plagioclase melting loop at 1 bar (Bowen 1913).

## 2 Structure of feldspars

In plagioclase feldspar there are four tetrahedral sites on which Al and Si atoms are distributed. The ordering process can be envisaged as occurring in two stages with decreasing temperature. In the first stage the Al and Si are distributed over two t1 and two t2 sites within the structure (Fig. 1). The order parameter for this process, designated  $Q_t$ , following Carpenter and Salje (1994), can be defined as

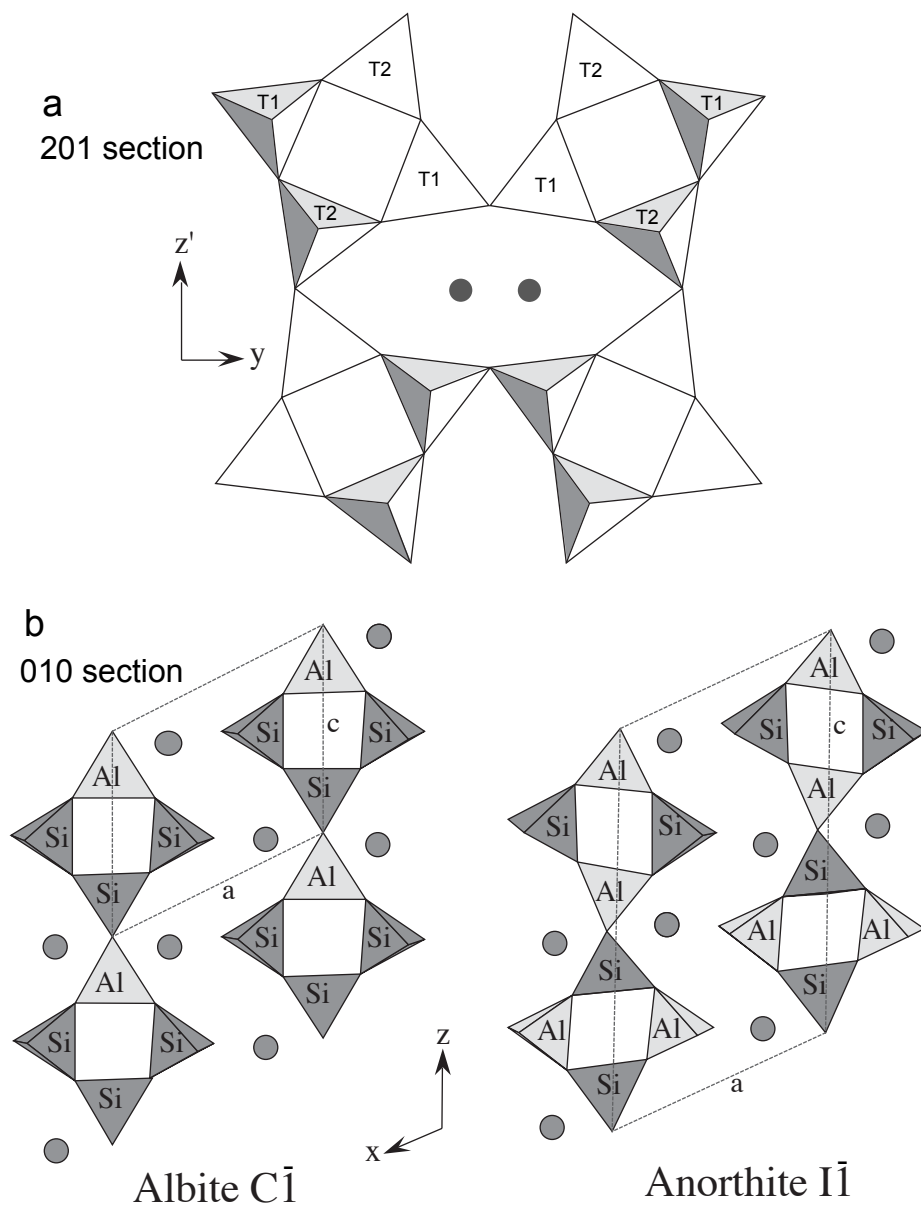
$$Q_t = \frac{X_{Al}^{t1} - X_{Al}^{t2}}{X_{Al}^{t1} + X_{Al}^{t2}} \quad (1)$$

and varies smoothly with decreasing temperature. As temperatures decrease a second stage in ordering occurs in which the t1 site splits into t1o and t1m sites. In practice these two processes probably proceed together and a second order parameter  $Q_{od}$  is required to monitor this further ordering behaviour. This may be defined as

$$Q_{od} = \frac{X_{Al}^{t1o} - X_{Al}^{t1m}}{X_{Al}^{t1o} + X_{Al}^{t1m}} \quad (2)$$

The thermodynamics of albite, K-feldspar and anorthite, individually, have been handled in terms of two such order parameters in Holland & Powell (1996), but not as yet together in ternary feldspars. Here, below, following Holland & Powell (1996), the order parameter definitions adopted omit the normalisations (the denominators) in equations 1 and 2, so

69  $Q_t = X_{Al}^{t1} - X_{Al}^{t2}$  and  $Q_{od} = X_{Al}^{t1o} - X_{Al}^{t1m}$ .



70  
 71 **Fig. 1.** Structure of feldspars illustrating the t1 and t2 tetrahedral sites and positions of the large cations  
 72 Ca, Na and K (circles). (a): (201) section showing 4-member rings of t sites; (b): (010) section showing  
 73 albite and anorthite ordering schemes with the unit cell a and c edges and the doubling of the c cell  
 74 dimension in anorthite.

75 The nature of order-disorder in the plagioclase solid solution permits various  
 76 phenomena that might have a significant impact on the thermodynamics of mixing. The  
 77 C1-I1 transition appears to be first-order, and stable between ca. 800°C and the solidus

78 (Jin *et al.*, 2018). A model containing the  $Q_t$  and  $Q_{od}$  parameters should in principle be  
79 intrinsically capable of modelling the transition, although, in our “2Q” model (see below),  
80 we did not succeed in producing such a transition. Other structural phenomena seen in  
81 plagioclase are not intrinsic to a model containing  $Q_t$  and  $Q_{od}$ , and it is not clear how they  
82 could be directly modelled. One is the strong tendency towards the reduction of Al–O–Al  
83 linkages (Al-avoidance; e.g. Kerrick & Darken, 1975), which introduces a short-range order,  
84 equating to a reduction in the configurational entropy contribution from tetrahedral-site  
85 mixing. Another is the incommensurately-ordered (aperiodic) structures taken on by  
86 intermediate-composition plagioclases, known as *e*-plagioclases, which may be stable at up  
87 to 800°C (Jin *et al.*, 2020, and references therein).

### 88 **3 Thermodynamic models of feldspar**

89 Many different simple models have been considered and fitted to the experimental database  
90 outlined above in an attempt to find one that is acceptable for real-world petrological  
91 calculations. The models cover a range of assumptions regarding the tetrahedral sites on  
92 which mixing of Si and Al occurs, and a range of behaviours relating to short-range order  
93 on those sites, relating also to the  $\text{NaSi}(\text{CaAl})_{-1}$  and  $\text{KSi}(\text{CaAl})_{-1}$  substitutions. The effect  
94 of short-range order is to reduce the entropic contribution to the  $a$ - $x$  relationships. We  
95 accommodate the reduction with an empirical approach, introduced in Holland & Powell  
96 (1996), and outlined in Appendix 1 here. A model in the following list, for example 4T,  
97 becomes model 4TR when entropy reduction is invoked.

98 The non-ideal mixing in the  $a$ - $x$  relationships is chosen to be via an asymmetric van  
99 Laar model with an interaction energy  $W_{i,j}$  for each pair of end-members and an asymmetry  
100 parameter  $\alpha_i$  for each end-member (Holland & Powell 2003).

101 Seven mixing models were considered for the  $a$ - $x$  relationships. Of these models, 4, 5  
102 and 6 in the list below were further investigated using a variety of entropy reduction factors.  
103 The seven essential structures were:

104 1. Simple molecular mixing. This is a fully ordered model in which all tetrahedral

105 disorder is ignored and taken to be fixed by complete correlation with A-site Na-Ca  
106 occupancy, for example, as in Holland & Powell (2003).

- 107 2. A full ordering (2Q) model, as outlined above, involving the  $Q_t$  and  $Q_{od}$  order  
108 parameters.
- 109 3. 1Q model. This model can be thought of as a simplification of model 2, involving only  
110 t1-t2 ordering, implying that further t1m-t1o ordering, which is important only at  
111 more albitic compositions, may be ignored. In the case of complete order this model  
112 reduces to the 2T Al-avoidance model 4.
- 113 4. 2T model. This is the so-called Al-avoidance model of Kerrick & Darken (1975), in  
114 which Al and Si mix on only 2 of the four tetrahedral sites.
- 115 5. 4T model. This is the fully disordered plagioclase model in which complete disorder is  
116 assumed to occur on all 4 tetrahedral sites. Model 4TR is the preferred model, as  
117 discussed below.
- 118 6. Intermediate end-member model. This model involves an additional species, for  
119 example, midway between albite and anorthite, and may be formulated in a variety of  
120 ways depending on whether or not the T sites contribute to mixing.
- 121 7. Macroscopic ordering model. This involves introducing tetrahedral site ordering  
122 without specifying the sites or number of sites involved. For example, one possibility  
123 investigated involved mixing of  $AlSi_3$  and  $Al_2Si_2$  clusters on the T sites.

## 124 4 Calibration of models

125 Of the 7 models put forward above, models 1 and 4 were rejected on the basis of poorer fits  
126 to one or more of the main constraining datasets (cation exchange, ternary feldspar pairs,  
127 plagioclase melting loop), and models 3, 6 and 7 added complexity to calculations without  
128 providing better fits to the data. In this section we present results of the calibration of the  
129 4TR model, along with the 2Q model for comparison, as they are two of the

130 best-performing models. The 4TR model is our preferred model, involving complete  
131 disorder on the four T sites in feldspar, and the effect of short-range ordering approximated  
132 by reducing their entropic contribution by a factor of 4 ( $\theta = 4$  in Appendix 1).

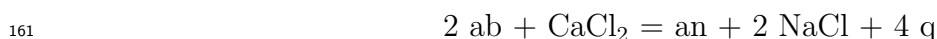
133 The 2Q model fully describes tetrahedral-site long-range ordering honouring the  
134 underlying order-disorder involving both the partition of Al and Si between the t1 and t2  
135 sites, and then the partition between the t1o and t1m sites that are present when the t1 site  
136 is split. Further details of the 2Q model are provided in Appendix 2.

137 Calibration of the new thermodynamic models involves using (a) the plagioclase  
138 cation-exchange experiments, (b) the alkali feldspar solvus, (c) experimental ternary  
139 feldspar pairs at 880 – 900°C, and (d) the dry melting loop for plagioclase at 1 bar. These  
140 are discussed in turn below. These data were fitted simultaneously using a Monte-Carlo  
141 approach in which pressure, temperature and feldspar compositions were calculated in  
142 THERMOCALC and filtered *via* brackets derived from the experimental studies. Model  
143 parameters were varied in the Monte-Carlo runs until 100 successful runs (those generating  
144 results within the filter brackets) were achieved (see Green *et al.*, 2016, p848, Holland *et al.*,  
145 2018). The experimental data used in fitting for the parameters of the plagioclase and melt  
146 model discussed above are listed in tables in Appendix 3. These tables comprise 36 sets of  
147 brackets (filters) for the Monte-Carlo runs.

148 On the basis of the calibration shown below, the 4TR model was selected as our  
149 preferred model, even though it is the 2Q model that explicitly represents order–disorder on  
150 the tetrahedral sites. The simplicity of the 4TR model recommends it over the 2Q model,  
151 given that its performance is no worse – indeed, somewhat better – than the 2Q model. We  
152 note that a good fit was achieved even though none of the models investigated represents  
153 the  $C\bar{I}-I\bar{I}$  transition, or an *e*-plagioclase structure, in any way. Apparently, these structural  
154 phenomena make an insignificant energetic contribution to phase equilibria, at least by  
155 comparison with the short-range order induced by Al-avoidance.

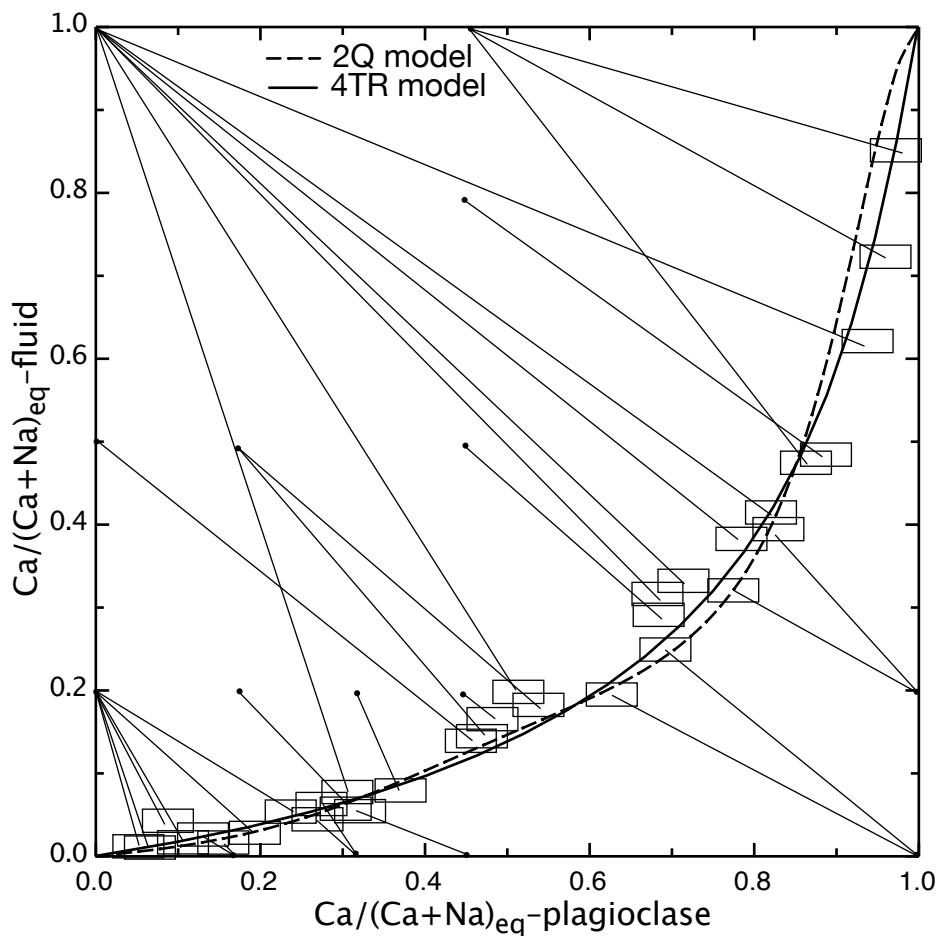
## 156 4.1 (a) Ca-Na cation exchange experiments

157 Orville (1972) and Schliestedt and Johannes (1990) presented experimental details of  
158 equilibrated pairs of plagioclase feldspar and NaCl–CaCl<sub>2</sub> fluid at 2 kilobars pressure at  
159 700°C and 600°C, and used the following exchange reaction to deduce the activities of albite  
160 and anorthite.



162 Brackets (see Appendix 3) from the experimental data shown in Fig. 2 were used for  
163 calibration, together with the assumption of ideal mixing in the aqueous fluid phase  
164 ( $a_{\text{NaCl}} = m_{\text{NaCl}}$ ,  $a_{\text{CaCl}_2} = m_{\text{CaCl}_2}$ ). This assumption is justified *a posteriori* by the  
165 satisfactory agreement with the other experimental data for plagioclase and ternary  
166 feldspars discussed below. The results are expressed in Ca/(Ca+Na) equivalent units (i.e.  
167  $2\text{Ca}/(2\text{Ca}+\text{Na})$ ) as discussed in Orville (1972) in order to compare with his diagram. As  
168 may be seen in Fig. 2, the cation exchange is closely approximated by the calculated  
169 models, except for small departures at high  $X_{\text{an}}$  with the 2Q model. It should be  
170 remembered that rather few experiments are true reversals using crystalline starting  
171 compositions, and those only at Ca-poor compositions. In addition, only compositions less  
172 than  $X_{\text{an}} = 0.82$  were approached from both directions. Brackets from Schliestedt &

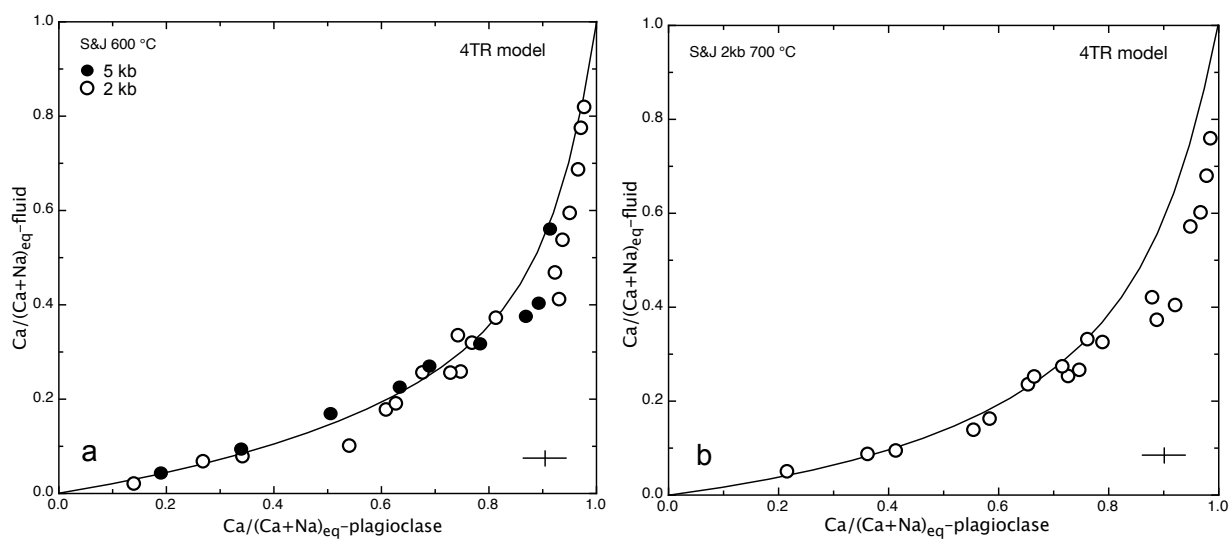
173 Johannes (1990) at 600°C and 2 and 5 kbar were also used in the Monte-Carlo analysis.



174  
175 **Fig. 2.** Experimental Ca-Na cation-exchange data for plagioclase–fluid at 700°C (boxes, Orville 1972) and  
176 calculated curves for the 2Q and 4TR models. Thin lines join starting and final compositions. Error boxes  
177 approximated as slightly smaller than those of Schliestedt and Johannes (1990) to reflect the smaller data  
178 scatter.

179 The experiments of Schliestedt and Johannes (1990) are slightly more scattered and  
180 displaced to slightly higher Ca contents of plagioclase at any fluid composition (Fig. 3) than  
181 those of Orville (1972), although possibly within combined experimental uncertainties, and  
182 are slightly less consistent with all the other data fitted simultaneously in the Monte-Carlo  
183 analysis. As shown in Fig. 3 and noted by Schliestedt and Johannes (1990) their data at  
184 2kb, 700°C, 2kb, 600°C and 5 kb, 600°C show the virtually identical exchange behaviour.

185 However they allow the model calibration to extend down to 600°C.



186 **Fig. 3.** Experimental Ca-Na cation-exchange data for plagioclase–fluid at 600°C (a) and at 700°C (b).  
187 Data of Schliestedt and Johannes (1990) and calculated curves for the 4TR model. Calculated curves at 2  
188 kb and 5 kb are coincident within error. Size of error bar from Schliestedt and Johannes (1990).

## 189 4.2 (b) Alkali feldspar solvus experiments

190 The alkali feldspar solvus was modelled previously by Holland & Powell (2003) and the  
191 parameters used there were taken as starting points in this study. Brackets at 2 kbar and  
192 550, 600, 650°C (Luth & Tuttle 1966, Orville 1963) and at 14-15 kbar and 500, 550, 600°C  
193 (Goldsmith & Newton 1974) were used in the Monte-Carlo runs to ensure consistency with  
194 the other experimental constraints discussed below. The fit

195 ( $W_{ab\ san} = 24.1 - 0.00957T + 0.338P (\pm 0.2)$  kJ,  $\alpha_{ab} = 0.674 (\pm 0.02)$ , with  $\alpha_{san}$  set at 1.0)  
196 differs slightly from that presented in Holland & Powell (2003) but the calculated solvi are  
197 almost indistinguishable from Fig. 3 in that work. In the case of the 2Q model, the  
198 calculated solvus is the same as for the 4TR model, but using the  $W$  and  $\alpha$  values given in  
199 Appendix 3 involving the three albite end-members and disordered sanidine.

### 4.3 (c) Ternary feldspar equilibration experiments of Elkins & Grove (1990)

The ternary feldspar system has been investigated extensively by Ghiorso (1984), Green & Usdansky (1986), Fuhrmann & Lindsley (1988) and Elkins & Grove (1990), using the Margules formulation for mixing energetics. Elkins & Grove (1990) analyzed their experimental results in the range 700–900°C with a one-site entropy of mixing and a subregular solution. In Holland & Powell (2003) the solution model also used a one-site entropy of mixing model in demonstrating the applicability of the van Laar and DQF approach, whereas we here use a reduced-entropy tetrahedral site model as described above.

The four experimental tie line pairs shown joining the grey composition regions in Fig. 4 (at 1 kbar and around 900°C) were taken in the Monte-Carlo fitting, together with pairs at 1 and 2 kbar at 800°C. As may be seen, for the 4TR model the calculated tie lines are slightly less steep at high Ca contents than implied by the experimental data, although it should be noted that the earlier work of Seck (1971) has slopes similar to the 4TR calculated ones. The 2Q model performs somewhat less well than that 4TR model, yielding still less steep tielines.

The 4TR model plagioclase solid solution parameters are

$$W_{ab\ an} = 14.6 - 0.00935T - 0.04P (\pm 0.3) \text{ kJ}$$

$$W_{ab\ or} = 24.1 - 0.00957T + 0.338P (\pm 0.2) \text{ kJ}$$

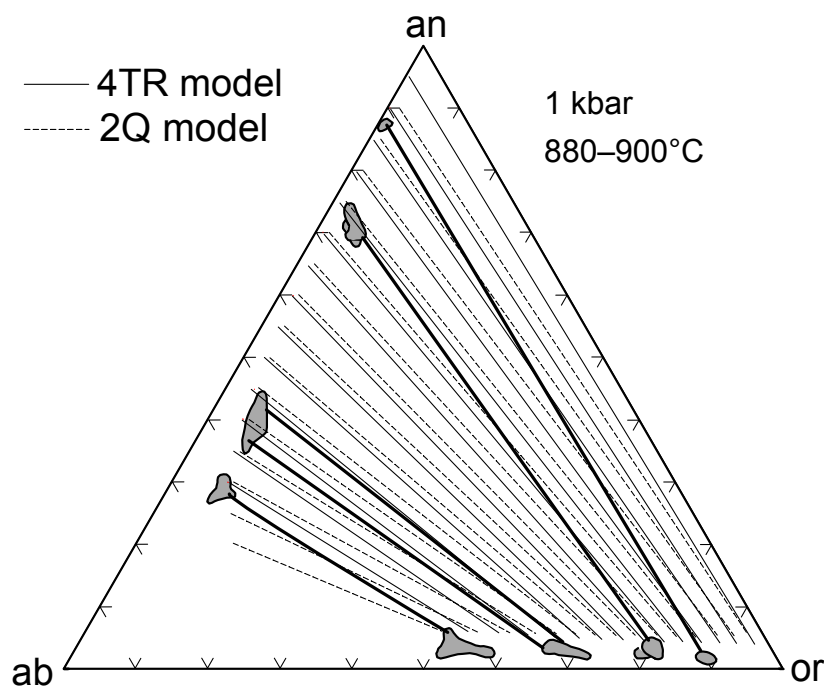
$$W_{an\ or} = 48.5 - 0.13P (\pm 0.5) \text{ kJ}$$

$$\alpha_{ab} = 0.674 (\pm 0.002)$$

$$\alpha_{an} = 0.550 (\pm 0.003)$$

$$\alpha_{or} = 1.00 \text{ (fixed)}$$

The uncertainties given above are just those that come from the ranges consistent with the filters in the Monte-Carlo fitting. They represent merely a guide to likely magnitudes, in the context of the essentially unquantifiable underlying model assumptions.



222

223 **Fig. 4.** Ternary feldspar relations at 1 kbar and 880–900°C. Grey fields are experimental  
 224 plagioclase–K-feldspar pairs with tie lines (heavy lines) from Elkins & Grove (1990). Tie lines joining  
 225 plagioclase and K-feldspar (light lines) are calculated.

#### 226 4.4 (d) Binary plagioclase melting at 1 bar of Bowen (1913)

227 Experimental data from Bowen (1913) on binary plagioclase melting were also used in the  
 228 Monte-Carlo analysis as additional constraints on the model. Pairs of coexisting plagioclase  
 229 and melt at 1120, 1200, 1300, 1400, 1500 and 1552°C were used as constraints. To ensure  
 230 correct melting temperatures for pure albite and pure anorthite, Gibbs free energy  
 231 increment parameters ( $\Delta G_{\text{anL}}^{\text{mod}}$  and  $\Delta G_{\text{abL}}^{\text{mod}}$ ) were also determined along with a symmetric  
 232 (regular solution) mixing parameter ( $W_{\text{anL abL}}$ ) for melt.

233 The calculated melting loop is shown in Fig. 5 compared with the experiments of  
 234 Bowen (1913). The agreement is good for both liquid and plagioclase compositions,  
 235 especially considering the difficulties of equilibration in dry feldspar melting experiments,  
 236 and hence in obtaining appropriate plagioclase compositions (Johannes *et al.* 1995). The  
 237 performance of the 4TR model is marginally better than that of the 2Q model.

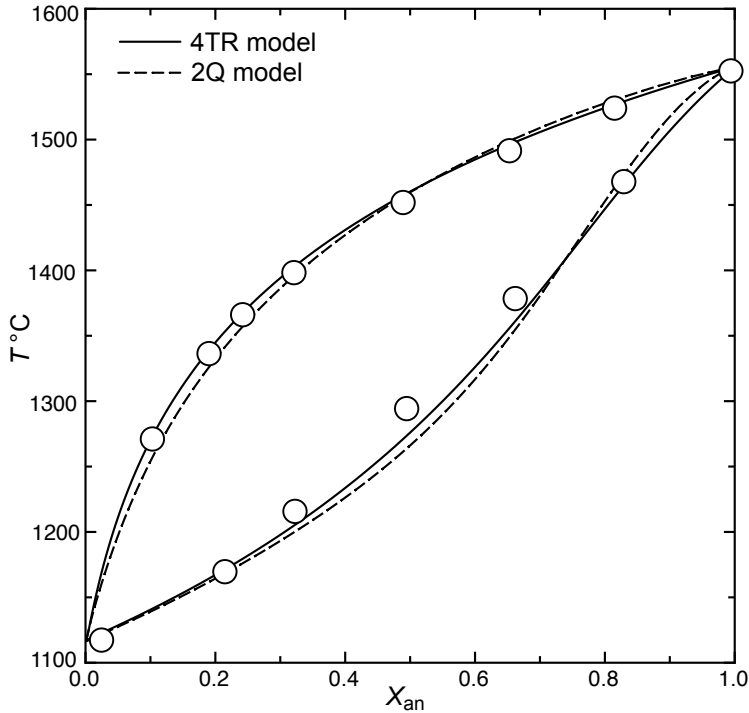
238 The abL–anL melt mixing parameters are

$$W_{\text{anL abL}} = 2.2 (\pm 0.2) \text{ kJ}$$

239  $\Delta G_{\text{abL}}^{\text{mod}} = -0.15 (\pm 0.2) \text{ kJ}$

$$\Delta G_{\text{anL}}^{\text{mod}} = 0.50 (\pm 0.2) \text{ kJ}$$

240 As in the earlier work of Holland & Powell (2001) anorthite–albite melt is found to be a  
241 nearly ideal solution.



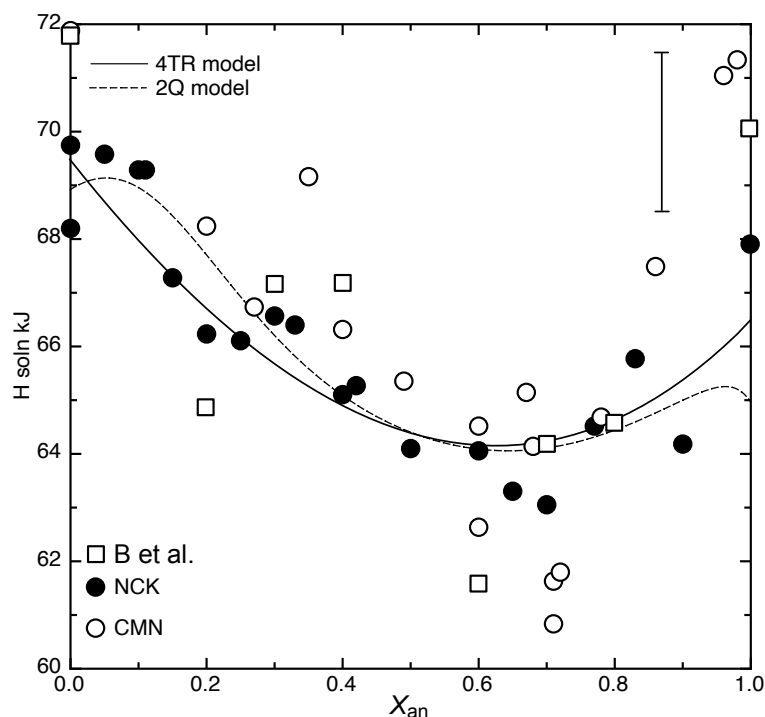
242  
243 **Fig. 5.** Plagioclase melting loop at 1 bar. Circles are experimental results of Bowen (1913). Curves are  
244 calculated with the 4TR and 2Q models.

## 245 5 Testing and application of the 4TR model

246 The 4TR model described and calibrated above is consistent with a wide range of  
247 experimental data over a range in temperature from 600–1550°C, suggesting that this  
248 entropy model and associated non-ideal mixing terms is appropriate for calculations for a  
249 wide range in rock formation conditions. We have left two experimental studies from our  
250 fitting in order to provide a check on the consistency of the model. The studies involve

251 calorimetric data on enthalpy of mixing in plagioclase and displaced-activity phase  
252 equilibrium experiments involving plagioclase at high pressures.

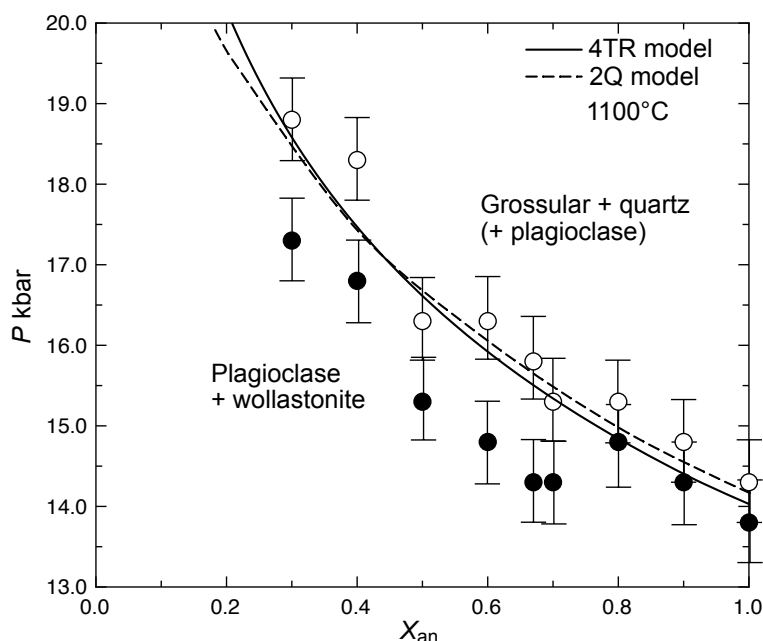
253 Newton *et al.* (1980) and Carpenter *et al.* (1985) provide enthalpy of solution data for  
254 plagioclases equilibrated at high temperatures (1100–1400°C) and run in a high-temper-  
255 ature solution calorimeter at 970K. As a test of the 4TR model we present a comparison of  
256 the calculated enthalpy of solution in Fig. 6 where the model compares favourably with the  
257 calorimetric data within its relatively large scatter. There appears to be slightly better  
258 agreement with the Newton *et al.* (1980) data perhaps because the model and their  
259 calorimetry are both based on synthetic plagioclases.



260  
261 **Fig. 6.** Plagioclase enthalpy of solution data from Newton *et al.* (1980), shown as black circles and the  
262 calculated 4TR and 2Q model curves for comparison. Open circles are heat-treated samples of Carpenter *et*  
263 *al.* (1985). Open squares are data of Benisek *et al.* (2003). Calculated values for albite and anorthite are  
264 arbitrarily taken as 69.5 and 66.5 kJ respectively. Vertical bar shows average error for experimental points.

265 As a final test, the experimental data of Windom & Boettcher (1976) on plagioclases  
266 equilibrated with wollastonite + grossular + quartz at 1100°C are compared with the 4TR  
267 model calculation. Figure 6 shows the experimental pressure brackets with the 4TR model

268 providing a reasonable fit to the experimental data. In Fig. 7 the experimental pressures  
 269 have been adjusted by -0.7 kbar such that the pressure for pure an + wo = gr + q agrees  
 270 with Windom & Boettcher's brackets, because the Holland & Powell (2011) dataset yields a  
 271 pressure of 14 kbar at that temperature. This corresponds to a 5% friction correction and is  
 272 typical of those applied to piston-cylinder experiments. The good agreement with the  
 273 plagioclase trend in  $X_{an}$  from 0.3 to 1.0 at pressures of 15–20 kbar suggest that the  
 274 plagioclase model is reliable through the pressure range of plagioclase stability.



275  
 276 **Fig. 7** Experimental determination of plagioclase compositions coexisting with grossular, wollastonite &  
 277 quartz from Windom & Boettcher (1976). Circles with error bars are experimental brackets, and the curves  
 278 are calculated with the 4TR and 2Q models.

279 The 4TR (and the 2Q) model predict increasing non-ideality with decreasing  
 280 temperature, which, at low temperatures, leads to a miscibility gap which closes at about  
 281 260°C and widens to lower temperature (Fig. 8). It is not meaningful to compare this  
 282 calculated gap with either the Hüttenlocher or Bøggild gaps, as neither any stable regions of  
 283 *e*-plagioclase nor the  $C\bar{I}-\bar{I}\bar{I}$  transition have been taken into account here.

284 In metabasic systems in particular, the peristerite gap is an important feature,  
 285 especially in the greenschist to amphibolite facies transition. In order to simulate a

286 peristerite gap, we introduce a low albite feldspar with properties that yield a narrow  
 287 peristerite-like gap at very low  $X_{an}$  and which closes at around 600°C (e.g. Carpenter 1981,  
 288 Nord *et al.* 1978). The mixing properties of the low albite solid solution involve a simple  
 289 1-site entropy of mixing and the parameters below. These generate a first order transition  
 290 at 600°C and the miscibility gap shown in Fig. 8, and considerably widen the miscibility  
 291 gap between albite and plagioclase at low temperatures. As discussed in Nord *et al.* (1978)  
 292 and Starr and Pattison (2019), whether the miscibility gap is a solvus or a binary loop is  
 293 unresolved; our model assumes the latter.

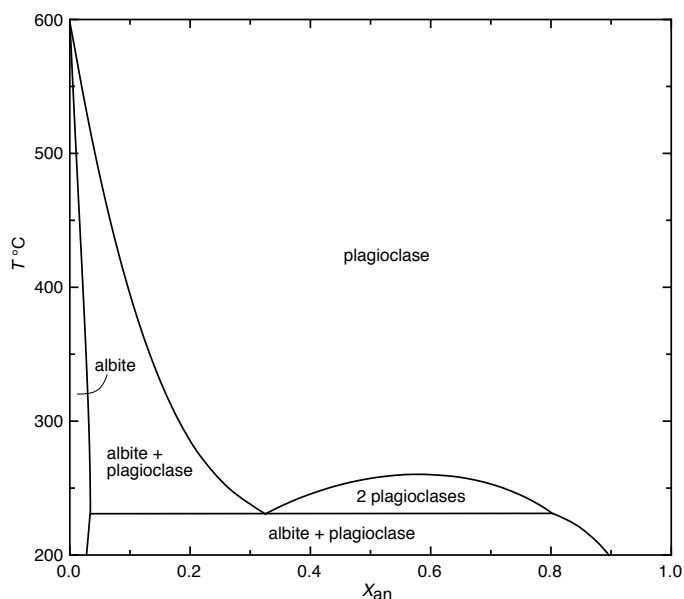
$$W_{an\ ab} = 3.4 (\pm 0.3) \text{ kJ}$$

$$\alpha_{an} = 1.00 \text{ (fixed)}$$

$$294 \quad \alpha_{ab} = 0.64 (\pm 0.02)$$

$$\Delta G_{ab}^{\text{mod}} = -1.746 + 0.002T (\pm 0.05) \text{ kJ}$$

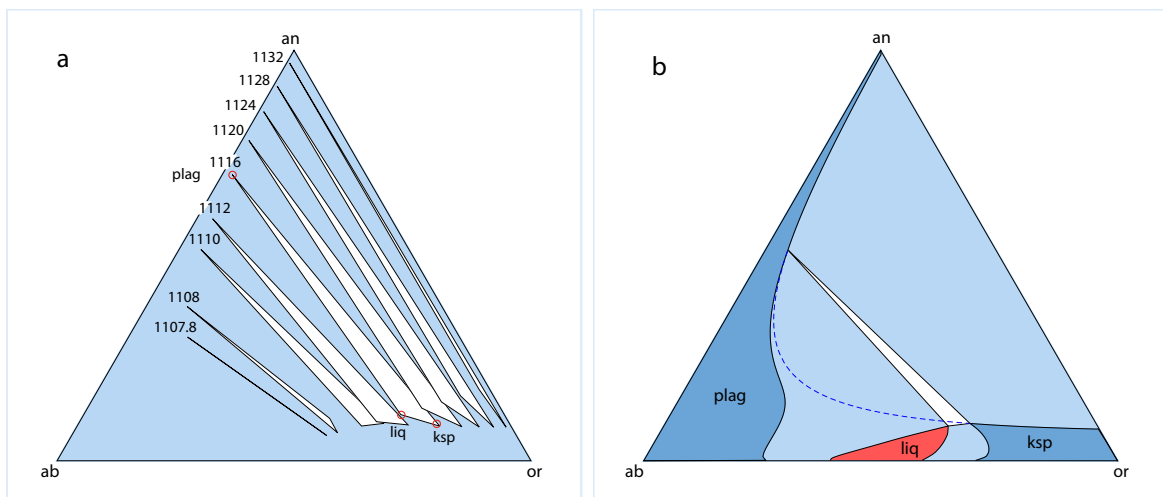
$$\Delta G_{an}^{\text{mod}} = 10.00 (\pm 0.05) \text{ kJ}$$



295  
 296 **Fig. 8.** Calculated  $T$ - $X_{an}$  section, showing the miscibility gap below around 260°C and the model  
 297 peristerite gap at very low  $X_{an}$  separating almost pure albite from an-rich plagioclase at lower temperature.  
 298  
 299 The calculated solvus relations below 300°C, even if predicted correctly, are metastable with

300 respect to *e*-plagioclase and the phase relationships associated with the Hüttenlocher and  
301 Bøggild gaps.

302 A simple example of the application of the feldspar model is to investigate the melting  
303 relationships of quartzofeldspathic rocks in the absence of H<sub>2</sub>O. Given the difficulty of  
304 determining metamorphic temperatures for UHT rocks, the dry melting relationships  
305 provide an effective upper temperature limit of crustal metamorphism, considered in terms  
306 of the metamorphism of broadly granitic rocks. Calculations in the system  
307 CaO – Na<sub>2</sub>O – K<sub>2</sub>O – Al<sub>2</sub>O<sub>3</sub>–SiO<sub>2</sub>, with quartz and sillimanite in excess, can be projected  
308 onto the ternary feldspar compatibility diagram, ab–an–or. Dry melting in ab–or starts at an  
309 azeotropic point at 1105°C and then spreads rapidly into the interior of the ternary feldspar  
310 triangle. By 1108°C there is a pl–ksp–liq tie triangle. With temperature increase, this tie  
311 triangle swings up and across towards the an–or side of the diagram (Fig. 9a). This shows  
312 that for normal granitic crustal compositions the upper limit of crustal metamorphic  
313 temperatures is 1100°C. Figure 9b shows the phase relationships at 1110°C. In the presence  
314 of even a small amount of H<sub>2</sub>O in the bulk composition of a granitic rock, melting will  
315 occur at markedly lower temperature than 1100°C. For example, at  $a_{\text{H}_2\text{O}} = 0.05$ , the  
316 equivalent position of the pl–ksp–liq tie triangle in (b) is 1025°C.



317  
318 **Fig. 9.** The 4TR model ternary diagrams, with excess sillimanite and quartz, at 8 kbar. (a) Migration of  
319 the 2-feldspar + liquid triangle with temperature (in °C). The lowest temperature “tie triangle”, essentially  
320 a colinear relationship between the phases, marks the temperature at which liq breaks through the feldspar

321 one-phase field into the body of the ab-an-or triangle, via a singular reaction. The positions of plag, liq and  
322 ksp at 1116°C are highlighted to show relative locations. (b) Showing phase relations of feldspars and liquid  
323 at 1110°C.

## 324 6 Discussion and Conclusions

325 Although the full order-disorder 2Q model is shown to be in reasonable agreement with  
326 experimental constraints, the simpler 4TR model can satisfy them as well, if not better.  
327 Both models omit the  $C\bar{I}$ – $I\bar{I}$  transition, and the presence of intermediate-composition  
328 *e*-plagioclase (whether stable or metastable). However, there is no clear evidence in  
329 calibration data that these phenomena significantly affect the results of the  
330 lower-temperature experiments. They appear to have only small consequences for the  
331 thermodynamics of the solid solution.

332 The plagioclase *a*–*x* relations of Holland & Powell (1992) explicitly represented the  
333  $C\bar{I}$ – $I\bar{I}$  transition, by having a separate thermodynamic model for each structure. Given that  
334 at least above 800°C, the  $C\bar{I}$ – $I\bar{I}$  transition is a line in a *T*-*x* diagram (not a 2-phase field),  
335 the separate thermodynamic models were made to be contiguous at the transition. Holland  
336 & Powell (2003) extended this approach into the ternary feldspar system. We now realise  
337 that it is not possible to make this extension into ternary feldspars without breaking the  
338 contiguity constraints, resulting in complex coexisting feldspar relations as an unwanted  
339 artefact. The new 4TR feldspar model can be seen as a replacement for the Holland &  
340 Powell (2003) model, which appropriately if implicitly represents the entropic consequences  
341 of configurational order-disorder. Like its predecessor, it is suitable for use in petrological  
342 phase equilibrium calculations along with version 6 of the Holland & Powell dataset  
343 (Holland & Powell, 2011), and associated families of activity-composition relations (White  
344 *et al.*, 2014; Green *et al.*, 2016; Holland *et al.*, 2018). The new plagioclase model should  
345 produce results that differ inconsequentially from the earlier models, but obviates the need  
346 to decide on whether the calculated plagioclase is  $C\bar{I}$  or  $I\bar{I}$  and removes any small  
347 disconnects or artificial  $C\bar{I}$ – $I\bar{I}$  coexisting feldspar pairs. The plagioclase of Tomlinson &

348 Holland (2021) is based on model 6 of this study and, while it should produce similar  
349 results, the new 4TR model presented here is recommended.

## 350 **Acknowledgements**

351 We thank Richard White for conversations about activity-composition relations, and the  
352 reviewers, Nicolas Riel and Jacob Forshaw, for their helpful comments and suggestions.

## References

- Benisek, A., Kroll, H., Cemic, L., Kohl, V., Breit, U. & Heying, B. 2003. Enthalpies in (Na,Ca)- and (K,Ca)-feldspar binaries: a high-temperature solution calorimetric study. *Contributions to Mineralogy and Petrology*, 145, 119–129.
- Benisek, A., Dachs, E. & Kroll, H. 2010. A ternary feldspar-mixing model based on calorimetric data: development and application. *Contributions to Mineralogy and Petrology*, 160, 327–337.
- Bowen, N.L. 1913. The melting phenomena of the plagioclase feldspars. *American Journal of Science*, 35(210), 577–599.
- Carpenter M.A. 1981. A “conditional spinodal” within the peristerite miscibility gap of plagioclase feldspars. *American Mineralogist*, 66, 553–560.
- Carpenter, M.A. & McConnell, J.D.C. 1984. Experimental delineation of the  $C\bar{I}-I\bar{I}$  transformation in intermediate plagioclase feldspars. *American Mineralogist*, 69, 112–121.
- Carpenter, M.A., & Salje, E.K.H 1994. Thermodynamics of nonconvergent cation ordering in minerals: III. Order parameter coupling in potassium feldspar. *American Mineralogist*, 79, 1084–1098
- Carpenter, M.A., McConnell, J.D.C. & Navrotsky, A. 1985. Enthalpies of ordering in the plagioclase feldspar solid solution. *Geochimica et Cosmochimica Acta*, 49, 947–966.
- Carpenter, M.A. 1994. Subsolidus phase-relations of the plagioclase feldspar solid-solution. In: Ian Parsons (Ed.) *Feldspars and their reactions*. Springer, Dordrecht, pp 221–269.
- Elkins, L.T. & Grove, T.L. 1990. Ternary feldspar experiments and thermodynamic models. *American Mineralogist*, 75, 544–559.
- Fuhrman, M.L. & Lindsley, D.H. 1988. Ternary feldspar modeling and thermometry. *American Mineralogist*, 73, 201–215.

- 378 Ghiorso, M.S. 1984. Activity/composition relations in the ternary feldspars. *Contributions*  
379 *to Mineralogy and Petrology*, 87, 282–296
- 380 Goldsmith J.R. & Newton R.C. 1974. An experimental determination of the alkali feldspar  
381 solvus. In: The Feldspars (ed WS MacKenzie & J Zussman). Manchester University  
382 Press.
- 383 Green, N.L. & Usdansky, S.T. 1986. Ternary feldspar relations and feldspar  
384 thermobarometry. *American Mineralogist*, 71, 1100–1108.
- 385 Green, E.C.R., White, R.W., Diener, J.F.A., Powell, R., Holland, T.J.B. & Palin, R.M.  
386 2016. Activity?composition relations for the calculation of partial melting equilibria in  
387 metabasic rocks. *Journal of Metamorphic Geology*, 34, 845–869.
- 388 Holland, T.J.B. & Powell, R., 1985. An internally consistent thermodynamic dataset with  
389 uncertainties and correlations: 2. Data and results. *Journal of Metamorphic Geology*,  
390 3, 343–370.
- 391 Holland, T.J.B. & Powell, R., 1990. An internally-consistent thermodynamic dataset with  
392 uncertainties and correlations: the system  
393 Na<sub>2</sub>O-K<sub>2</sub>O-CaO-MgO-MnO-FeO-Fe<sub>2</sub>O<sub>3</sub>-Al<sub>2</sub>O<sub>3</sub>-SiO<sub>2</sub>-TiO<sub>2</sub>-C-H<sub>2</sub>-O<sub>2</sub>. *Journal of*  
394 *Metamorphic Geology*, 8, 89–124.
- 395 Holland T.J.B. & Powell R. 1992. Plagioclase feldspars: activity-composition relations  
396 based upon Darken's quadratic formalism and Landau theory. *American Mineralogist*,  
397 77, 53–61
- 398 Holland, T. J. B. & Powell, R. 1996. Thermodynamics of order-disorder in minerals: 1.  
399 Symmetric formalism applied to minerals of fixed composition. *American*  
400 *Mineralogist*, 81, 1413–1424.
- 401 Holland, T.J.B., & Powell, R. 1998. An internally-consistent thermodynamic dataset for  
402 phases of petrological interest. *Journal of Metamorphic Geology*, 16, 309–344.

- 403 Holland, T. J. B. & Powell, R. 2001. Calculation of phase relations involving haplogranitic  
404 melts using an internally-consistent thermodynamic dataset. *Journal of Petrology*, 42,  
405 673–683.
- 406 Holland, T.J.B., & Powell, R. 2003. Activity–composition relations for phases in  
407 petrological calculations: an asymmetric multicomponent formulation. *Contributions*  
408 *to Mineralogy and Petrology*, 145, 492–501.
- 409 Holland, T.J.B. & Powell, R. 2011. An improved and extended internally consistent  
410 thermodynamic dataset for phases of petrological interest, involving a new equation of  
411 state for solids. *Journal of Metamorphic Geology*, 29, 333–383.
- 412 Holland, T.J., Green, E.C.R. & Powell, R. 2018. Melting of peridotites through to  
413 granites: a simple thermodynamic model in the system KNCFMASHTOCr. *Journal*  
414 *of Petrology*, 59, 881–900.
- 415 Jin, S. & Xu, H. 2017. Investigations of the phase relations among e1, e2 and  $C\bar{1}$   
416 structures of Na-rich plagioclase feldspars: a single-crystal X-ray diffraction study.  
417 *Acta Crystallographica Section B: Structural Science, Crystal Engineering and*  
418 *Materials*, 73, 992–1006.
- 419 Jin, S., Wang, X. & Xu, H. 2018. Revisiting the  $I\bar{1}$  structures of high-temperature Ca-rich  
420 plagioclase feldspar—a single-crystal neutron and X-ray diffraction study. *Acta*  
421 *Crystallographica Section B: Structural Science, Crystal Engineering and Materials*,  
422 74, 152–164.
- 423 Jin, S., Xu, H., Wang, X., Zhang, D., Jacobs, R. & Morgan, D. 2019. The  
424 incommensurately modulated structures of volcanic plagioclase: displacement,  
425 ordering and phase transition. *Acta Crystallographica Section B: Structural Science,*  
426 *Crystal Engineering and Materials*, 75, 643–656.
- 427 Jin, S., Xu, H., Wang, X., Zhang, D., Jacobs, R. & Morgan, D. 2020. The  
428 incommensurately modulated structures of low-temperature labradorite feldspars: a

- 429 single-crystal X-ray and neutron diffraction study. *Acta Crystallographica Section B:*  
430 *Structural Science, Crystal Engineering and Materials*, 76, 93–107.
- 431 Johannes, W. Koepke, J. & Behrens, H. 1994. Partial Melting Reactions of Plagioclases  
432 and Plagioclase-Bearing Systems. In *Feldspars and Their Reactions* (Ed: Ian  
433 Parsons). Springer, Dordrecht, Netherlands 161–194.
- 434 Kerrick, D.M. & Darken, L.S. 1975. Statistical thermodynamic models for ideal oxide and  
435 silicate solid solutions, with applications to plagioclase. *Geochimica et Cosmochimica*  
436 *Acta*, 39, 1431-1442.
- 437 Luth, W.C. & Tuttle O.F. 1966 The alkali feldspar solvus in the system  
438  $\text{Na}_2\text{O}-\text{K}_2\text{O}-\text{Al}_2\text{O}_3-\text{SiO}_2-\text{H}_2\text{O}$ . *American Mineralogist*, 51, 1359–1373.
- 439 McConnell, J.D.C. 2008. The origin and characteristics of the incommensurate structures  
440 in the plagioclase feldspars. *The Canadian Mineralogist* 46, 1389–1400.
- 441 Newton, R.C., Charlu, T.V. & Kleppa, O.J. 1980. Thermochemistry of the high structural  
442 state plagioclases. *Geochimica et Cosmochimica Acta*, 44, 933–941.
- 443 Nord, G. L., Jr., Hammarstrom, J. L., & Zen, E-An. 1978. Zoned plagioclase and  
444 peristerite formation in phyllites from south-western Massachusetts. *American*  
445 *Mineralogist*, 63, 947–955.
- 446 Orville, P.M. 1963. Alkali ion exchange between vapor and feldspar phases. *American*  
447 *Journal of Science*, 261, 201–237.
- 448 Orville, P.M. 1972. Plagioclase cation exchange equilibria with aqueous chloride solution:  
449 results at 700°C and 200 bars in the presence of quartz. *American Journal of Science*,  
450 272, 234–272.
- 451 Powell, R., & Holland, T.J.B. 1993. On the formulation of simple mixing models for  
452 complex phases *American Mineralogist* 78, 1174–1180.

- 453 Schliestedt, M. & Johannes, W. 1990. Cation exchange equilibria between plagioclase and  
454 aqueous chloride solution at 600 to 700°C and 2 to 5 kbar. *European Journal of*  
455 *Mineralogy*, 2, 283–295.
- 456 Spear, F.S. (1977). Evidence for a miscibility gap in plagioclase feldspar in the composition  
457 range An<sub>33</sub>–An<sub>88</sub>. *Carnegie Institution of Washington Yearbook*, 76, 619–621.
- 458 Starr, P.G. & Pattison, D.R.M. 2019. Equilibrium and disequilibrium processes across the  
459 greenschist–amphibolite transition zone in metabasites. *Contributions to Mineralogy*  
460 *and Petrology*, 174, 1–18.
- 461 Tomlinson, E.L. & Holland, T.J.B. 2021. A Thermodynamic Model for the Subsolidus  
462 Evolution and Melting of Peridotite. *Journal of Petrology*, 62, 1–23.
- 463 Wenk, H.-R. 1979. An albite-anorthite assemblage in low-grade amphibolite facies rocks.  
464 *American Mineralogist*, 64, 1294–1299.
- 465 Wenk, E. & Wenk, H.-R. 1977. An-variation and intergrowths of plagioclases in banded  
466 metamorphic rocks from Val Carrechio (Central Alps). *Schweizerische Mineralogische*  
467 *und Petrographische Mitteilungen*, 57, 41–57.
- 468 White, R.W., Powell, R., Holland, T.J.B., Johnson, T.E. & Green, E.C.R. 2014. New  
469 mineral activity?composition relations for thermodynamic calculations in metapelitic  
470 systems. *Journal of Metamorphic Geology*, 32, 261–286.
- 471 Windom, K.E. & Boettcher, A.L. 1976. The effect of reduced activity of anorthite on the  
472 reaction grossular + quartz = anorthite + wollastonite: a model for plagioclase in the  
473 earth's lower crust and upper mantle. *American Mineralogist*, 61, 889–896.

## 474 Appendix 1: Simulation of short-range ordering

475 The reduction of the entropy of mixing to simulate the effect of local, or short-range,  
476 ordering is an empirical device introduced in Holland & Powell (1996) for spinel Mg-Al  
477 ordering and Holland & Powell (1998) for amphiboles, and has been used widely in  $a$ - $x$   
478 modelling since then, e.g. White *et al.* (2014). Such entropy reduction is illustrated here  
479 using the 2T and 4T models (see text) for plagioclase. First, for the 2T model

$$480 \begin{aligned} a_{\text{an}}^{\text{ideal}} &= x_{\text{Ca,A}} (x_{\text{Al,TB}}^2) \\ a_{\text{ab}}^{\text{ideal}} &= 4^{\frac{1}{\theta}} x_{\text{Na,A}} (x_{\text{Al,TB}} x_{\text{Si,TB}}) \end{aligned}$$

481 Now consider a 2TR model (R meaning reduced entropic contribution), with the entropic  
482 contribution of the tetrahedral sites to be reduced by a factor,  $\theta$ . With  $\theta > 1$ , this amounts  
483 to asserting that the  $\text{NaSi}(\text{CaAl})_{-1}$  coupled substitution exerts an additional short-range  
484 effect, on top of that provided by Al avoidance.

$$485 \begin{aligned} a_{\text{an}}^{\text{ideal}} &= x_{\text{Ca,A}} (x_{\text{Al,TB}}^2)^{\frac{1}{\theta}} \\ a_{\text{ab}}^{\text{ideal}} &= 4^{\frac{1}{\theta}} x_{\text{Na,A}} (x_{\text{Al,TB}} x_{\text{Si,TB}})^{\frac{1}{\theta}} \end{aligned}$$

486 In these expressions the TB sites are the sites that admit Al and Si and the pre-factor  
487 for ab is a normalisation constant. In the simple 2T (or Al-avoidance) model,  $\theta = 1$ . If  $\theta$  is  
488 large the ideal mixing activities reduce to those of molecular mixing, as used in Holland &  
489 Powell (2003), with  $a_{\text{an}}^{\text{ideal}} = x_{\text{Ca,A}}$ ,  $a_{\text{ab}}^{\text{ideal}} = x_{\text{Na,A}}$ , and  $a_{\text{san}}^{\text{ideal}} = x_{\text{K,A}}$ . The magnitude of  $\theta$  for  
490 any model to successfully explain the experimental data is related to the entropy of mixing  
491 in the model.

492 For the 4T model

$$493 \begin{aligned} a_{\text{ab}}^{\text{ideal}} &= \left(\frac{256}{27}\right) x_{\text{Na,A}} (x_{\text{Al,T}} x_{\text{Si,T}}^3) \\ a_{\text{an}}^{\text{ideal}} &= x_{\text{Ca,A}} (x_{\text{Al,T}}^2 x_{\text{Si,T}}^2) \end{aligned}$$

494 Now consider a 4TR model, with the entropic contribution of the tetrahedral sites to be  
495 reduced by a factor,  $\theta$ . The ideal mixing activities are then:

$$496 \begin{aligned} a_{\text{ab}}^{\text{ideal}} &= \left(\frac{256}{27}\right)^{\frac{1}{\theta}} x_{\text{Na,A}} (x_{\text{Al,T}} x_{\text{Si,T}}^3)^{\frac{1}{\theta}} \\ a_{\text{an}}^{\text{ideal}} &= x_{\text{Ca,A}} (x_{\text{Al,T}}^2 x_{\text{Si,T}}^2)^{\frac{1}{\theta}} \end{aligned}$$

497 As noted in the text, the 4TR model is the only one that fits all of the experimental  
498 constraints well, and involves complete disorder on the four T sites in feldspar (see text)  
499 and with  $\theta = 4$ . Then, the ideal mixing activities for ab, an and or are:

$$a_{\text{ab}}^{\text{ideal}} = \left(\frac{256}{27}\right)^{\frac{1}{4}} x_{\text{Na,A}} (x_{\text{Al,T}} x_{\text{Si,T}}^3)^{\frac{1}{4}}$$

$$a_{\text{or}}^{\text{ideal}} = \left(\frac{256}{27}\right)^{\frac{1}{4}} x_{\text{K,A}} (x_{\text{Al,T}} x_{\text{Si,T}}^3)^{\frac{1}{4}}$$

$$a_{\text{an}}^{\text{ideal}} = x_{\text{Ca,A}} (x_{\text{Al,T}}^2 x_{\text{Si,T}}^2)^{\frac{1}{4}}$$

## 501 Appendix 2: The 2Q model

502 The end-members used, in terms of the A, t1o, t1m and t2 sites in the 2Q model, are

503	A			t1o		t1m		t2		
504	Na	Ca	K	Al	Si	Al	Si	Al	Si	
505	oab	1	0	0	1	0	0	1	0	2
506	dab	1	0	0	1/4	3/4	1/4	3/4	1/2	3/2
507	oan	0	1	0	1	0	1	0	0	2
508	tab	1	0	0	1/2	1/2	1/2	1/2	0	2
509	san	0	0	1	1/4	3/4	1/4	3/4	1/2	3/2

510 where oab and dab are ordered and disordered albite, tab is t1-t2 ordered albite, oan is  
 511 ordered anorthite, and san is disordered sanidine. With the 4 independent variables

$$\begin{aligned}
 x &= X_{\text{Ca}}^{\text{A}} \\
 k &= X_{\text{K}}^{\text{A}} \\
 512 \quad Q_{\text{t}} &= \frac{X_{\text{Al}}^{\text{t1o}} + X_{\text{Al}}^{\text{t1m}}}{2} - X_{\text{Al}}^{\text{t2}} \\
 Q_{\text{od}} &= X_{\text{Al}}^{\text{t1o}} - X_{\text{Al}}^{\text{t1m}}
 \end{aligned}$$

513 Note that these expressions for the order parameters are different from those of Carpenter  
 514 & Salje (1994) in equations 1 and 2 in that the normalisation in the denominators is  
 515 missing, as noted in the text. This difference is not relevant to the thermodynamic analysis.  
 516 and site fractions

$$\begin{aligned}
 X_{\text{Na}}^{\text{A}} &= 1 - k - x \\
 517 \quad X_{\text{Ca}}^{\text{A}} &= x \\
 X_{\text{K}}^{\text{A}} &= k
 \end{aligned}$$

$$X_{\text{Al}}^{\text{t1o}} = \frac{1}{4} + \frac{1}{2}Q_{\text{od}} + \frac{1}{2}Q_{\text{t}} + \frac{1}{4}x$$

$$X_{\text{Si}}^{\text{t1o}} = \frac{3}{4} - \frac{1}{2}Q_{\text{od}} - \frac{1}{2}Q_{\text{t}} - \frac{1}{4}x$$

$$X_{\text{Al}}^{\text{t1m}} = \frac{1}{4} - \frac{1}{2}Q_{\text{od}} + \frac{1}{2}Q_{\text{t}} + \frac{1}{4}x$$

$$X_{\text{Si}}^{\text{t1m}} = \frac{3}{4} + \frac{1}{2}Q_{\text{od}} - \frac{1}{2}Q_{\text{t}} - \frac{1}{4}x$$

$$X_{\text{Al}}^{\text{t2}} = \frac{1}{4} - \frac{1}{2}Q_{\text{t}} + \frac{1}{4}x$$

$$X_{\text{Si}}^{\text{t2}} = \frac{3}{4} + \frac{1}{2}Q_{\text{t}} - \frac{1}{4}x$$

519 and end-member proportions  $p_{\text{oab}} = Q_{\text{od}}$ ,  $p_{\text{dab}} = 1 - k + x - Q_{\text{t}}$ ,  $p_{\text{oan}} = x$ ,

520  $p_{\text{tab}} = -Q_{\text{od}} + Q_{\text{t}} - 2x$ ,  $p_{\text{san}} = k$

521 and ideal mixing activities

$$a_{\text{oab}} = X_{\text{Na}}^{\text{A}} X_{\text{Al}}^{\text{t1o}} X_{\text{Si}}^{\text{t1m}} (X_{\text{Si}}^{\text{t2}})^2$$

$$a_{\text{dab}} = \frac{256}{27} X_{\text{Na}}^{\text{A}} (X_{\text{Al}}^{\text{t1o}})^{\frac{1}{4}} (X_{\text{Si}}^{\text{t1o}})^{\frac{3}{4}} (X_{\text{Al}}^{\text{t1m}})^{\frac{1}{4}} (X_{\text{Si}}^{\text{t1m}})^{\frac{3}{4}} (X_{\text{Al}}^{\text{t2}})^{\frac{1}{2}} (X_{\text{Si}}^{\text{t2}})^{\frac{3}{2}}$$

$$a_{\text{oan}} = X_{\text{Ca}}^{\text{A}} X_{\text{Al}}^{\text{t1o}} X_{\text{Al}}^{\text{t1m}} (X_{\text{Si}}^{\text{t2}})^2$$

$$a_{\text{tab}} = 4 X_{\text{Na}}^{\text{A}} (X_{\text{Al}}^{\text{t1o}})^{\frac{1}{2}} (X_{\text{Si}}^{\text{t1o}})^{\frac{1}{2}} (X_{\text{Al}}^{\text{t1m}})^{\frac{1}{2}} (X_{\text{Si}}^{\text{t1m}})^{\frac{1}{2}} (X_{\text{Si}}^{\text{t2}})^2$$

$$a_{\text{san}} = \frac{256}{27} X_{\text{K}}^{\text{A}} (X_{\text{Al}}^{\text{t1o}})^{\frac{1}{4}} (X_{\text{Si}}^{\text{t1o}})^{\frac{3}{4}} (X_{\text{Al}}^{\text{t1m}})^{\frac{1}{4}} (X_{\text{Si}}^{\text{t1m}})^{\frac{3}{4}} (X_{\text{Al}}^{\text{t2}})^{\frac{1}{2}} (X_{\text{Si}}^{\text{t2}})^{\frac{3}{2}}$$

523 and non-ideal mixing terms via van Laar model (in kJ)

$$W(\text{oab}, \text{dab}) = 11 + 0.04P$$

$$W(\text{oab}, \text{oan}) = 19.2 + 0.35P$$

$$W(\text{oab}, \text{tab}) = 5.4 + 0.04P$$

$$W(\text{oab}, \text{san}) = 30.4 + 0.365P$$

$$W(\text{dab}, \text{oan}) = 40.8 + 0.34P$$

$$W(\text{dab}, \text{tab}) = 0.6 + 0.04P$$

$$W(\text{dab}, \text{san}) = 12.2 + 0.365P$$

$$W(\text{oan}, \text{tab}) = 8 + 0.27P$$

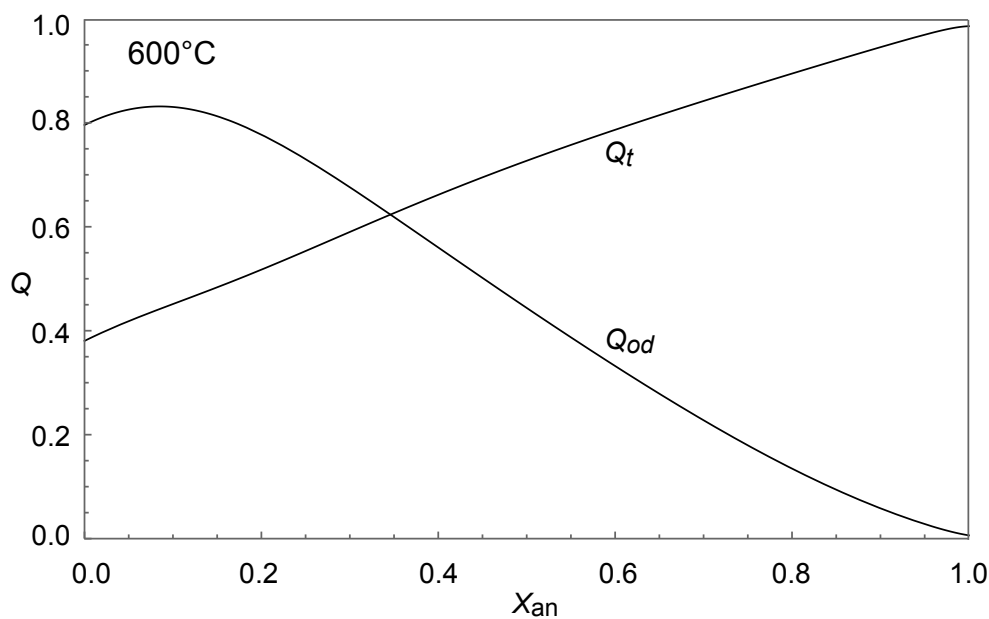
$$W(\text{oan}, \text{san}) = 77.1 - 0.093P$$

$$W(\text{tab}, \text{san}) = 14.4 + 0.365P$$

525 and the Gibbs energies of the end-members are taken to be: san = sanidine, oab = ordered  
526 albite, oan = ordered anorthite, tab = ordered albite +15.17 - 0.011526T + 0.04P (kJ), dab

527 = ordered albite  $+18.12 - 0.018702T + 0.04P$  (kJ). Asymmetry parameters are:  $\alpha(\text{san}) =$   
528 1.00,  $\alpha(\text{oan}) = 0.667$ ,  $\alpha(\text{oab}) = \alpha(\text{dab}) = \alpha(\text{tab}) = 0.685$ .

529 In the 2Q model there are two internal equilibria that need to be solved to determine  
530 the state of order— $Q_t$  and  $Q_{od}$ —for any composition of feldspar. These internal equilibria  
531 are  $\Delta\mu = 0$  equations for each of the independent reactions between the end-members, for  
532 example,  $\text{oab}=\text{dab}$  and  $\text{oab}=\text{tab}$ . Figure A2.1 shows the variation of  $Q_t$  and  $Q_{od}$  at 600°C  
533 in plagioclase, solving the internal equilibria, and using the parameters listed above. At  
534 high anorthite contents, the feldspar is almost completely ordered onto the t1 and t2 sites  
535 with no ordering onto the t1o and t1 m sites, while at albitic compositions the t1 and t2 are  
536 approximately half ordered and there is a high degree of ordering onto the to1 and t1m  
537 sites, as expected.



538  
539 **Fig. A2.1.** Calculated variation of  $Q_t$  and  $Q_{od}$  with plagioclase composition at 600°C for the 2Q model.

540 **Appendix 3: Data used in fitting**

541 **1. Orville (1972) cation exchange, 2 kbar 700°C**

	$X_{Ca,pl}$	$Ca/(Ca + Na)_{fl}$
1	0.12–0.16	0.025
2	0.24–0.28	0.053
3	0.39–0.44	0.11
542 4	0.54–0.59	0.18
5	0.74–0.83	0.33
6	0.94–0.98	0.74
7	0.38	0.08–0.12

543 Where pl and fl refer to plagioclase and fluid.

544 **2. Ternary feldspars, Elkins & Grove (1990)**

	$X_{Ca,pl}$	$X_{K,pl}$	$X_{Ca,ksp}$	$X_{K,ksp}$	$P$ kbar	$T$ °C
8	0.33–0.50	0.018–0.09	0.01–0.04	0.75	2	800
9	0.31–0.46	0.022–0.09	0.01–0.04	0.73	2	800
10	0.30–0.43	0.025–0.13	0.01–0.04	0.71	2	800
545 11	0.38–0.46	0.025–0.10	0.01–0.049	0.67	1	800
12	0.24–0.33	0.06–0.12	0.02–0.057	0.56	1	890
13	0.72–0.76	0.0085–0.05	0.01–0.045	0.82	1	900
14	0.85–0.91	0.0027–0.05	0.01–0.041	0.89	1	890
15	0.10–0.16	0.10–0.20	0.01–0.05	0.45	1	800

546 **3. Alkali feldspar solvus: 2kb Orville, (1963), Luth & Tuttle (1966); 14 kb**  
547 **Goldsmith & Newton (1974)**

	$X_{K,ab}$	$X_{K,ksp}$	$P$ kbar	$T^{\circ}C$
16	0.05–0.10	0.69–0.75	2	550
17	0.07–0.14	0.60–0.67	2	600
548 18	0.14–0.21	0.47–0.56	2	650
19	0.01–0.05	0.87–0.93	14	500
20	0.02–0.06	0.84–0.91	14	550
21	0.02–0.08	0.79–0.85	14	600

549 **4. Plagioclase melting loop, Bowen (1913)**

	$X_{Ca,L}$	$X_{Ca,pl}$	$P$ kbar	$T^{\circ}C$
22	0.04–0.07	0.27–0.34	0.001	1200
23	0.12–0.17	0.48–0.55	0.001	1300
550 24	0.31–0.34	0.68–0.73	0.001	1400
25	0.62–0.72	0.84–0.93	0.001	1500
26	0.0–0.02	0.0–0.05	0.001	1118
27	0.94–1.00	0.98–1.00	0.001	1551

551 **5. Schliestedt & Johannes (1990) cation exchange**

	$X_{\text{Ca,pl}}$	$\text{Ca}/(\text{Ca} + \text{Na})_{\text{fl}}$	$T^{\circ}\text{C}$	$P$ kb
28	0.91–0.98	0.62	700	2
29	0.80–0.90	0.40	700	2
30	0.58–0.64	0.20	700	2
31	0.91–0.98	0.62	600	2
32	0.72–0.82	0.30	600	2
33	0.47–0.55	0.15	600	2
34	0.32–0.40	0.10	600	5
35	0.56–0.64	0.20	600	5
36	0.78–0.85	0.38	600	5

552  
553 Where pl and fl refer to plagioclase and fluid.